Available online at www.sciencedirect.com
SCIENCE DIRECT®
Journal of Nuclear Materials 324 (2004) 97–115
journal of nuclear materials
www.elsevier.com/locate/jnucmat

Modelling the alteration gel composition of simplified borosilicate glasses by precipitation of an ideal solid solution in equilibrium with the leachant

I. Munier [a,*], J.-L. Crovisier [a], B. Grambow [b], B. Fritz [a], A. Clément [a]

[a] *Ecole et Observatoire des Sciences de la Terre, Centre de Géochimie de la Surface, ULP, CNRS, Strasbourg, France*
[b] *Ecole des Mines, SUBATECH, Nantes, France*

Received 1 August 2002; accepted 26 August 2003

Abstract

The modelling of the alteration process of two model glasses (Si–Al–B–Na and Si–Al–B–Na–Ca–Zr), having the same molar ratio as the French reference SON68 glass, with the geochemical code KINDIS was studied. The formation of the alteration layer was simulated by the precipitation of an ideal solid solution. This simulation study was compared then with the alteration experiments carried out in parallel: glasses were placed at 363 K in pure water at two different S/V ratios (1 and 80 cm^{-1}) for duration of 30–180 days. The thermodynamic stability of the siliceous end-members of the solid solution has a fundamental influence on the simulation results. Thus, with suitable end-members (chalcedony and hydroxides), the simulation allows one to reproduce with a good agreement the evolution of the silicon content in solution as well as the chemical composition of the gel layer. The experimental results and the simulations seem to indicate a control of the gel composition over the glass dissolution process.

PACS: 81.05.Kf; 82.20.Wt; 82.30.−b; 82.60.Lf

1. Introduction

The question of the long-term disposal of nuclear waste has greatly stimulated the study of glass weathering. The researches were focused on glasses (basalt glasses essentially) considered as natural analogues of nuclear glasses [1–7] as well as on the R7T7 borosilicate (SON68) glass, used as the French confinement matrix for the light water reactor (LWR) high level nuclear waste [2,8,9].

The dissolution process of these glasses can be decomposed into three successive phases. The first step corresponds to an ion exchange coupled to a hydration process, which leads to the release of alkali metal and alkaline earth cations and to the formation of a leached and hydrated glass surface region [10,11,82]. During this step, the water-soluble glass network formers, such as boron, together with the alkali elements are mobilised and released: the process is governed by diffusion in the pore space of the still existing glass network. The glass constituents are then released incongruently, because the rate of alkali and boron release is much faster than that of silicon. Simultaneously, the glass network becomes hydrolysed, leading to a disintegration of the glassy state and to the dissolution of the glass network constituents such as Si or Al. Once the network hydrolysis rate

* Corresponding author. Now at ANDRA Agence Nationale pour la Gestion, des Déchets Radioactifs, Direction Scientifique/Service Intégration, Parc de la Croix Blanche, 1-7 rue Jean Monnet, 92298 Châtenay Malabry, France. Tel.: +33-1 46 11 81 07; fax: +33-1 46 1184 08.
E-mail address: isabelle.munier@andra.fr (I. Munier).

0022-3115/$ - see front matter © 2003 Elsevier B.V. All rights reserved.
doi:10.1016/j.jnucmat.2003.08.033

becomes faster than the alkali/boron diffusion rate, the dissolution becomes congruent (second step). At the third step, secondary alteration products (the amorphous gel and mineral phases) form and the glass dissolution becomes incongruent again [2,3,8,9,12–28]. As the reaction proceeds, the glass matrix dissolution rate decreases, due to the accumulation of dissolved glass constituents in the solution. As a consequence, the extent of glass hydrolysis is less important at high than at a low sample surface to solution volume ratio (S/V) whereas the relative importance of ion exchange increases with increasing S/V.

Quantifying these processes requires the use of a mathematical model for simulating long-term glass alteration. Two main types of processes were simulated until now: the formation of secondary products and the dissolution kinetics.

The development of geochemical models has helped greatly the simulation of alteration products formation during glass dissolution. As applied to basaltic and nuclear glasses, these programs (EQ3/6, GLASSOL, KINDIS...) allow one to simulate the sequence of precipitation of minerals [3,18,25,27,29–35,78,80,81]. However, they do not take into account the formation of the amorphous alteration gel nor the kinetic aspect of glass dissolution. The goal of the present article is to model the formation of the gel that is the first stage toward a kinetic modelling.

The kinetic equations usually used to describe the dissolution of nuclear and basaltic glasses have been derived essentially from the general law proposed by Aagaard and Helgeson [36] concerning the dissolution of minerals and based on the transition state theory. This kinetic law considers that the dissolution rate depends directly on the affinity of the rate limiting elementary reaction. One of the authors [37] has adapted this dissolution rate to silicate glasses by postulating that the limiting step of the glass dissolution is the desorption of a purely siliceous surface complex. The reaction rate is then expressed according to the activity of the orthosilicic acid in solution at saturation (Eq. (1)):

$$r = r_0\left(1 - \frac{a(\mathrm{H_4SiO_4})}{a(\mathrm{H_4SiO_4})_{\mathrm{sat}}}\right) \quad \text{and} \quad r_0 = k(a(H^+))^n, \qquad (1)$$

with r_0, the initial dissolution rate; $a(\mathrm{H_4SiO_4})$, the orthosilicic acid activity in solution; $a(\mathrm{H_4SiO_4})_{\mathrm{sat}}$, the orthosilicic acid activity at saturation with respect to the pristine glass; k the kinetic constant; $a(\mathrm{H^+})$ the proton activity in solution and n its stoichiometric coefficient in the rate limiting reaction.

Some authors considered that the activated complex controlling glass dissolution might be not purely siliceous and they adapted Eq. (1) by including other elements in the affinity calculations, such as Al or Fe [38–40]. Besides, the attempts to use the overall chemical affinity of the glass with respect to water as affinity control failed [35,41–43]. Other refinements have been considered, such as the reduction of the initial dissolution rate by an inhibiting effect of the orthosilicic acid on glass dissolution [35,42,44]. Thus, Bourcier et al. [45] have proposed a model, in which the dissolution rate depends on the affinity between the alteration gel, regarded as an ideal solid solution, and the solution rather than on the affinity between the glass and the solution. Many of these models have been assessed by using specific experimental data; however they failed to account for the totality of experimental results, especially when considering the long-term dissolution, where these models are far from reproducing the drop of the dissolution rate. The main reason for this failure is that the overall process of glass dissolution consists in a number of sequential and parallel reactions, with a rate limiting step changing with time. This is the case for the above-mentioned ion-exchange and hydrolysis processes, whose ratio of rates might be inverted again, provided that network hydrolysis will become slowed down by the reduced dissolution affinity. Furthermore, most models mentioned above do not take into account an important process occurring upon glass alteration: the precipitation of secondary compounds. The precipitation of these compounds can have two main consequences on the dissolution rate: either indirectly by modifying only the composition of the solution, and/or directly by influencing the dissolution process through the formation of mass transfer barriers to reactants (water) or to products (silicon, aluminium...). In the first case, the affinity equation remains valid, but affinity calculations have to be performed through geochemical codes to account for the change of the solution chemistry as the reaction proceeds. In the second case, if the reaction products form a mass transfer resistance to dissolved glass constituents, the affinity term applies only to the pore water at the interface between the glass phase and the reaction products. Then, the alteration layer would act as a diffusion barrier to siliceous species and the rate limiting step would be the diffusion rate. The influence of the gel layer on glass dissolution has been taken into account in affinity models [46–48,80,81]. These models were applied only on short-term dissolution and, with the exception of the model GLASSOL [80,81], ignored both the incidence of the gel formation on the chemical composition of the solution and the incidence of the formation of other secondary products on the dissolution process.

So as to be precise the influence of the formation and of the composition of the alteration gel on the solution chemistry, the aim of this study was to simulate the dissolution of glasses, analogues of nuclear glasses, and the alteration gel precipitation with the geochemical model KINDIS.

2. Experimental procedure

2.1. Glasses composition and experimental setup

Two model glasses (*glass 1*: Si–Al–B–Na and *glass 2*: Si–Al–B–Na–Ca–Zr) were studied, having the same elemental molar ratios as in the French SON68 nuclear glass. Details of glass making were reported in [73]; their chemical composition is given in Table 1.

The static alteration experiments were performed on a glass disk (diameter: 3 cm, thickness: 3 mm) with some glass powder sieved between 100 and 120 μm, in pure water at 363 (±1) K. The specific area of the glass powders was determined through the BET (krypton) method (*glass 1*: 663 cm^2/g, *glass 2*: 638 cm^2/g). The densities of the glasses were 2.405 and 2.500 g/cm^3 for glass 1 and glass 2 respectively. Two sets of experiments were carried out with two surface area of glass/volume of solution (S/V) ratios: 1 and 80 cm^{-1}.

Experiments were conducted in a Teflon vessel having undergone an ultra-clean washing protocol. The glass cylinder was placed into a small Teflon basket and immersed into the homogeneous solution. The glass powder remains on the bottom of the Teflon vessel without being stirred. The cylinder and powder were immersed into 100 cm^3 of preheated deionised water, then placed in oven during 30, 60, 90, 120, 150 and 180 days. After sampling, half of the solution was filtered to 0.2 μm by using a specially designed syringe and 1 cm^3 of bi-distilled nitric acid was added to the filtrate. Meanwhile, the pH was measured on the remaining fraction, which was thereafter filtered through 0.2 μm millipore filters as well. The glass cylinder was rapidly rinsed and let to dry at room temperature and the glass powder was dried at 363 K.

The boron content was analysed in the non-acidified fraction by Colorimetry (Technicon Autoanalyser II; siliconmolybdate method). The other elements (Si, Al, Na, Ca and Zr) were analysed in the acidified fraction by inductively coupled plasma-atomic emission spectrometry (ICP-AES, Jobin-Yvon JY 124) (accuracy $\leqslant 2\%$).

After coating with amorphous carbon, a portion of the glass cylinders was examined through analytical scanning electron microscopy (ASEM, JEOL JSM 804 link with an EDS detector Tracor TN 5500). The chemical composition of the alteration layer was analysed down to different depths by varying the acceleration tension of the incident beam between 4 and 30 kV. The measurements were carried out at a single spot. The sodium loss versus analysis time and acceleration tension was estimated by comparison with the sodium analysis in the pristine glass. This loss is linear and was then corrected. The chemical composition of the alteration layer was deduced from analyses at the weakest tensions, when the corrected sodium content remained constant.

The ultra-microtomic sections [49] of the glass powder were also observed and analysed through Analytical Scanning Transmission Electron Microscopy (ASTEM, Philips CM12 link with an EDS detector Tracor TN 5500).

2.2. Alteration parameters

The normalized mass loss (NL) (Eq. (2)) associated with an element '*i*' corresponds to the mass of glass altered by unit of surface area and is calculated from the element '*i*' concentration in solution.

$$\mathrm{NL}(i) = \frac{C(i)}{\mathrm{wt\%}(i) \cdot S/V}, \tag{2}$$

with $C(i)$, the concentration of element '*i*' in solution (μg/l); S/V, the ratio between the surface area of glass and the volume of the solution (cm^{-1}) (presumably constant during the experiment); wt%(i), the mass percentage of element '*i*' in the glass. NL(i) is expressed in g/m^2.

Table 1
Theoretical compositions of the two studied glasses in oxides wt%, in elemental molar%, and in oxides and metasilicates molar%

Oxides wt%	B_2O_3	Al_2O_3	SiO_2	Na_2O	CaO	ZrO_2
Glass 1	18.90	6.61	61.22	13.27	–	–
Glass 2	17.34	6.06	56.18	12.17	4.98	3.28
Molar%	B	Al	Si	Na	Ca	Zr
Glass 1	0.1227	0.0731	0.5984	0.2058	–	–
Glass 2	0.1080	0.0643	0.5267	0.1810	0.0714	0.0487
	B_2O_3	Al_2O_3	SiO_2	Na_2SiO_3	$CaSiO_3$	$ZrSiO_4$
Glass 1	0.2003	0.0478	0.5939	0.1580	–	–
Glass 2	0.2003	0.0478	0.5093	0.1579	0.0714	0.0133

In order to take into account a possible decrease of the glass surface, the surface variation was evaluated by using the 'shrinking core' model [85] adapted to our experimental conditions (glass powder and glass cylinder).

The average dissolution rate (R) of an element 'i' is calculated by means of the Eq. (3).

$$R(i) = \frac{\mathrm{NL}(i, t_{n+1}) - \mathrm{NL}(i, t_{n-1})}{t_{n+1} - t_{n-1}}, \tag{3}$$

where $R(i)$ is in $\mathrm{g\,m^{-2}\,d^{-1}}$ and the time (t) in days.

The thickness (T) of the altered glass is calculated from the normalized mass loss of boron (used as an alteration tracer) (Eq. (4)).

$$T(B) = \frac{\mathrm{NL}(B)}{\rho}, \tag{4}$$

with ρ, the glass density in g/cm^3.

2.3. Solid solution simulation

The simulation of the dissolution of the two model glasses was performed by using the geochemical code KINDIS [50–52]. This program allows one to calculate the speciation of the aqueous species and to simulate the irreversible dissolution of minerals and reversible precipitation of secondary phases. Two kinetic laws can be used: (i) an affinity law derived from the transition state theory corresponding to Grambow's model [37] (cf. introduction), with the orthosilicic acid in solution being considered as the only affinity controlling species (Eq. (1)), and (ii) a global affinity model, in which the overall affinity of the glass is considered [35,41–43]. By using KINDIS, the formation of complex minerals, such as clays or the alteration gel, can be simulated by a solid solution concept [53,54].

The free enthalpy ($G_{\mathrm{mech.}}$) of a mechanical mixture, including the same end-members with the same molar fractions (x_i) as in the case of an equivalent solid solution, can be then expressed [53].

$$G_{\mathrm{mech.}} = \sum_{i=1}^{i=p} x_i \mu_i^0(T), \tag{5}$$

with μ_i^0, the chemical potential of the solid 'i' and x_i, its molar fraction in the mixture; T, the temperature.

If we now consider a solid solution with 'p' end-members ($P_1 \ldots P_i \ldots P_p$) of molar fractions x_i, the chemical potential μ_i of end-member P_i in the solid solution is expressed by:

$$\mu_i = \mu_i^0(T) + RT\ln(A_i) \quad \text{and} \quad A_i = \gamma_i x_i, \tag{6}$$

with γ_i its activity coefficient; A_i, its activity; R, the ideal gas constant.

The free enthalpy ($G_{\mathrm{sol.}}$) of the solid solution thus comes:

$$G_{\mathrm{sol.}} = \sum_{i=1}^{i=p} x_i \mu_i(T,P) = \sum_{i=1}^{i=p} x_i \mu_i^0(T) + \sum_{i=1}^{i=p} x_i RT\ln(A_i), \tag{7}$$

with P, the pressure.

In the case of an ideal solid solution, where $\gamma_i = 1$, the mixing free enthalpy ($\Delta G_{\mathrm{mix.}}$) is then:

$$\Delta G_{\mathrm{mix.}} = G_{\mathrm{sol.}} - G_{\mathrm{mech.}} = RT \sum_{i=1}^{i=p} x_i \ln(x_i) \quad \text{and} \quad \Delta G_{\mathrm{mix.}} < 0. \tag{8}$$

This shows that an ideal solid solution is more stable, from a thermodynamic point of view, than the mechanical mixture of its end-members. However real solid solution formation may be limited thermodynamically by non-ideal mixing ($\gamma_i \neq 1$).

If we consider the equilibrium between the end-members P_i and their dissolved species (S_k) in the solution (case of an ideal solid solution) (Eq. (9)), the partial solubility products K_i and their molar fractions x_i are expressed as follows (Eq. (10) and (11)):

$$P_i \Longleftrightarrow v_{i1}S_1 + \cdots + v_{ik}S_k + \cdots + v_{in}S_n, \tag{9}$$

$$K_i = Q_i/A_i = \prod_k^n a_k^{v_{ik}}/A_i = \prod_k^n a_k^{v_{ik}}/\gamma_i x_i = \prod_k^n a_k^{v_{ik}}/x_i, \tag{10}$$

with K_i, the partial thermodynamic solubility product of the end-member P_i; Q_i, the ionic activity product of end-member P_i; a_k the activity of the aqueous species S_k in solution,

$$\text{and then } x_i = Q_i/K_i. \tag{11}$$

The condition for a solid solution to be at equilibrium with the solution is that each of its end-members is at equilibrium. It follows Eqs. (12)–(14) at equilibrium:

$$Q = \prod_{i=1}^{i=p} (Q_i)^{x_i} = \prod_{i=1}^{i=p} (K_i x_i)^{x_i} = K, \tag{12}$$

$$\ln K = \sum_i^p x_i \ln K_i + \sum_i^p x_i \ln x_i, \tag{13}$$

and

$$\Delta G_{\mathrm{diss}}^0 = \sum_i^p x_i \Delta G_{i,\mathrm{diss}}^0 - RT \sum_i^p x_i \ln x_i, \tag{14}$$

with Q, the global ionic activity product of the solid solution; K, the apparent overall solubility product;

ΔG^0_{diss}, the free enthalpy of dissolution of the solid solution; $\Delta G^0_{i,\text{diss}}$, the free enthalpy of dissolution of the end-member P_i.

Besides, the sum of the molar fractions of the solid solution end-members is equal to unity:

$$\sum_{i=1}^{i=p} x_i = \sum_{i=1}^{i=p} \frac{Q_i}{K_i} = 1. \tag{15}$$

This last relation, valid for an ideal solid solution, implies that the end-members are in equilibrium with the solution while their molar fraction is lower than 1 [53,54]. This state of saturation is then greatly different from what it is in the case of a pure end-member (where $x_i = 1$).

When considering solid solution formation, the KINDIS code calculates all the Q_i/K_i ratios and their sum as a function of reaction progress. When the sum of the Q_i/K_i ratios reaches unity, the solid solution is simulated to precipitate. The composition of the solid solution is then directly obtained from the Q_i/K_i ratios.

The choice of solid solution end-members used to represent the alteration gel and of their thermodynamic stability has an important influence on the simulated composition of the solution and of the gel. To quantify this influence, three types of solid solution, having oxides, hydroxides or metasilicates as end-members, were studied (Table 2). Besides, to account for the siliceous end-member thermodynamic stability, three different siliceous end-members were considered: quartz, chalcedony and amorphous silica.

2.4. Thermodynamic parameters calculation

Following Paul [55], the glasses were considered as a solid solution of oxides and metasilicates (Table 1). Their dissolution equation was written by taking into account the reference aqueous species of the KINDIS model: H_4SiO_4, $Al(OH)_4^-$, $B(OH)_3$, Na^+, Ca^{2+}, $Zr(OH)_4$, H_2O and H^+. Hence, for glasses 1 and 2 respectively:

$$\begin{aligned}&(B_2O_3)_{0.2003}(Al_2O_3)_{0.0478}(SiO_2)_{0.5939}(Na_2SiO_3)_{0.1580}\\&\quad + 2.1857H_2O + 0.2203H^+ \Longleftrightarrow 0.4006B(OH)_3\\&\quad + 0.0956Al(OH)_4^- + 0.7518H_4SiO_4 + 0.3160Na^+,\end{aligned}$$

and:

$$\begin{aligned}&(B_2O_3)_{0.2003}(Al_2O_3)_{0.0478}(SiO_2)_{0.5093}(Na_2SiO_3)_{0.1579}\\&\quad \times (CaSiO_3)_{0.0714}(ZrSiO_4)_{0.0133} + 2.1410H_2O\\&\quad + 0.3630H^+ \Longleftrightarrow 0.4006B(OH)_3 + 0.0956Al(OH)_4^-\\&\quad + 0.7519H_4SiO_4 + 0.3158Na^+ + 0.0714Ca^{2+}\\&\quad + 0.0133Zr(OH)_4.\end{aligned}$$

The solubility constants were then estimated by using the equation for ΔG^0_{diss} of a solid solution presented above (Eq. (14)). Thus, the free enthalpies of dissolution were calculated from the free enthalpy of formation of their components (Tables 1 and 3). The $\log K$ values at 363 K were estimated by using the Van't Hoff relation, simplified by neglecting the temperature dependence of the reaction enthalpy (Eq. (16) and (17)):

$$\frac{\partial \ln K^0_T}{\partial T} = \frac{\Delta H^0}{R_G T^2}, \tag{16}$$

and

$$\log K^0_T = \log K^0_{298} - \left(\frac{\Delta H^0_{298}}{2.303 R_G}\left(\frac{1}{T} - \frac{1}{298.15}\right)\right), \tag{17}$$

with K^0_T, the solubility constant of the reaction at temperature T (363.15 K); K^0_{298}, the solubility constant at 298.15 K; ΔH^0_{298}, the enthalpy of the reaction at 298.15 K (J mol^{-1}); and R_G, the ideal gas constant (8.314 $\text{J K}^{-1}\,\text{mol}^{-1}$).

The solubility constant of the two glasses were calculated (Eq. (14)), by using chalcedony as siliceous end-member:

$$\Delta G(\text{glass1}) = -6.18 + 3.22 = -2.96\ \text{kJ mol}^{-1},$$

$$\Delta G(\text{glass2}) = -11.04 + 4.07 = -6.97\ \text{kJ/mol}^{-1},$$

and thus $\log K$ (glass 1, 363 K) = 0.43 and $\log K$ (glass 2, 363 K) = 1.00.

These values compare well to those deduced from experimental measurement for a Si–Na–B–Al glass [56]. Indeed, considering our thermodynamic data for oxides dissolution and their measured free enthalpy of glass formation, the $\log K$ (363 K) of their glass is −0.71, which is of the same order of magnitude. Our glass 1

Table 2
End-members of the solid solutions considered in simulations (SiO_2: amorphous silica, chalcedony or quartz)

	Glass 1			Glass 2				
	Si	Al	Na	Si	Al	Na	Ca	Zr
Oxides	SiO_2	Al_2O_3	Na_2O	SiO_2	Al_2O_3	Na_2O	CaO	ZrO_2
Hydroxides	SiO_2	$Al(OH)_3$	NaOH	SiO_2	$Al(OH)_3$	NaOH	$Ca(OH)_2$	$Zr(OH)_4$
Metasilicates	SiO_2	Al_2O_3	Na_2SiO_3	SiO_2	Al_2O_3	Na_2SiO_3	$CaSiO_3$	$ZrSiO_4$

Table 3
Dissolution equations and free enthalpies of dissolution (kJ/mol) at 363 K

Dissolution equations	$\log K_{363\,K}$	$\Delta G_{\text{diss } 363\,K}$	Refs.
$SiO_{2am} + 2H_2O \iff H_4 \iff SiO_4$	−2.25	15.67	[57]
$SiO_{2chalcedony} + 2H_2O \iff H_4SiO_4$	−2.96	20.57	[57]
$SiO_{2quartz} + 2H_2O \iff H_4SiO_4$	−3.19	22.15	[57]
$H_4SiO_4 \iff H_3SiO_4^- + H^+$	−8.95		[53]
$Na_2O + 2H^+ \iff 2Na^+ + H_2O$	56.39	−391.7	[57,58]
$CaO + 2H^+ \iff Ca^{2+} + H_2O$	26.56	−184.5	[57]
$B_2O_3 + 3H_2O \iff 2B(OH)_3$	5.08	−35.32	[59,60]
$Al_2O_3 + 5H_2O \iff 2Al(OH)_4^- + 2H^+$	−24.54	170.50	[59,61]
$ZrO_2 + 2H_2O \iff Zr(OH)_{4aq}$	−11.6[a]	48.55[a]	[63,86]
$NaOH \iff Na^+ + OH^-$	6.87		[61]
$Ca(OH)_2 + 2H^+ \iff Ca^{2+} + 2H_2O$	18.63		[64,65]
$Al(OH)_3 + H_2O \iff Al(OH)_4^- + H^+$	−12.51		[53]
$Zr(OH)_{4c} \iff Zr(OH)_{4aq}$	−3.9[a]		[86,87]
$Na_2SiO_3 + 2H^+ + H_2O \iff 2Na^+ + H_4SiO_4$	17.75	−123.27	[55,61]
$CaSiO_3 + 2H^+ + H_2O \iff Ca^{2+} + H_4SiO_4$	8.83	−61.36	[55]
$ZrSiO_4 + 4H_2O \iff Zr(OH)_{4aq} + H_4SiO_4$	−17.76[a]	101.40[a]	[57,62,63,66,86]

[a] At 298 K.

composition being quite different from their Si–Na–B–Al glass composition, we used our calculated $\log K$.

3. Experimental results

3.1. Evolution of the elements concentration

The elements concentrations measured in the glass 1 leachates at 1 and 80 cm^{-1} have been reported in Table 4. The pH values stabilised after 60 days around 9, probably due to the buffer effect of boron. The final pH values were a little higher in the case of experiments at $S/V = 80$ cm^{-1} and consistent with the literature [67]. This difference may be due to the high contribution of the ion exchange process at high S/V ratio to the overall elements release. The concentrations of boron and sodium increased regularly (Fig. 1(a) and (b)); boron was released preferentially. For comparison, the boron concentration measured by [73] for the aqueous alteration of glass 1 in the same conditions at $S/V = 80$ cm^{-1} has been reported Fig. 1(b) and the agreement with our analysis is excellent. The ratio of alkali to silicon release increases with the S/V as expected from the higher relative importance of ion exchange at higher S/V. The silicon and aluminium concentrations increased and then stabilized after 90 days at $S/V = 1$ cm^{-1} and after 60 days at $S/V = 80$ cm^{-1} (Fig. 1(a) and (b)). The normalized mass losses (Eq. (2)) of the released glass constituents have been plotted on Fig. 2(a) and (b) (the

Table 4
Experimental results of the glass 1 static alteration at 1 and 80 cm^{-1} (363 K, pure water)

Days	pH	Concentration (mmol/l)				Normalized mass loss ($g\,m^{-2}$)			
		Si	Al	B	Na	NL(Si)	NL(Al)	NL(B)	NL(Na)
Glass 1, $S/V = 1$ cm^{-1}									
30	8.73	0.76	0.12	2.28	1.26	0.86	1.05	4.81	3.36
60	8.87	0.92	0.17	3.12	1.95	1.12	1.60	7.16	5.68
90	8.85	1.22	0.18	3.86	2.63	1.49	1.74	8.82	7.63
120	8.86	1.22	0.21	4.49	2.50	1.71	2.33	11.83	8.36
150	8.85	1.22	0.23	5.38	3.35	1.89	2.75	15.68	12.38
180	8.86	1.23	0.21	5.27	3.33	1.87	2.56	15.13	12.12
Glass 1, $S/V = 80$ cm^{-1}									
30	9.37	3.98	0.003	87.3	34.3	0.054	0.000	2.21	1.10
60	9.05	4.19	0.012	113.4	56.0	0.058	0.001	2.96	1.85
90	8.99	3.99	0.015	103.7	66.6	0.055	0.002	2.68	2.18
120	8.96	4.09	0.012	124.9	73.0	0.058	0.001	3.31	2.45
150	8.94	4.25	0.018	136.6	81.8	0.061	0.002	3.67	2.79
180	8.99	4.16	0.012	135.5	92.0	0.059	0.001	3.64	3.13

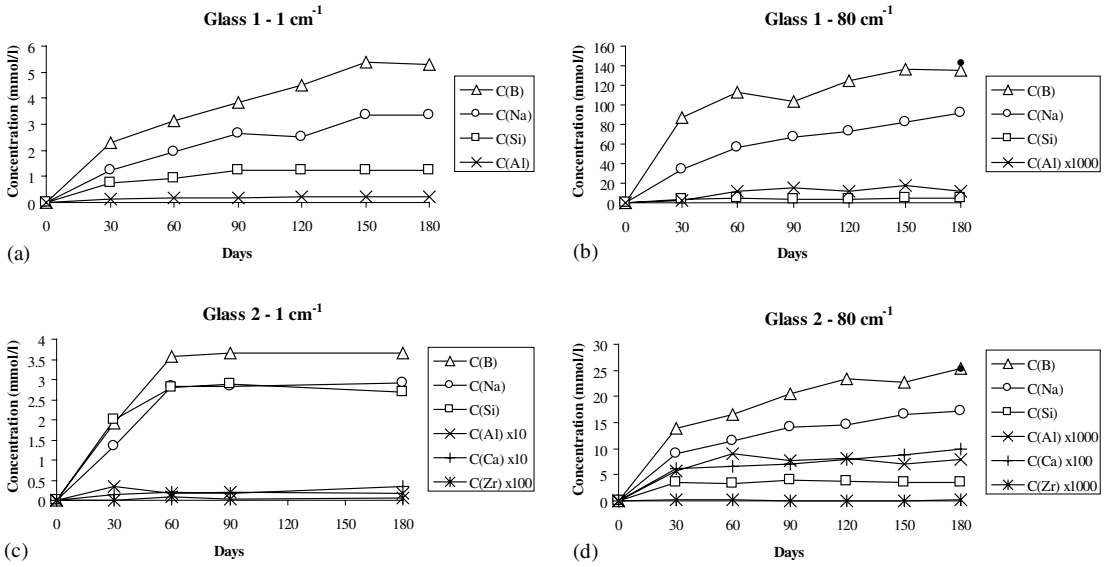

Fig. 1. Concentrations (mmol/l) versus time of the elements liberated by the glasses alteration in pure water at 363 K ((a) and (b): glass 1, (c) and (d): glass 2) (symbol size represents the uncertainty) (●: boron concentrations obtained by [73] for similar glasses altered six months, for comparison).

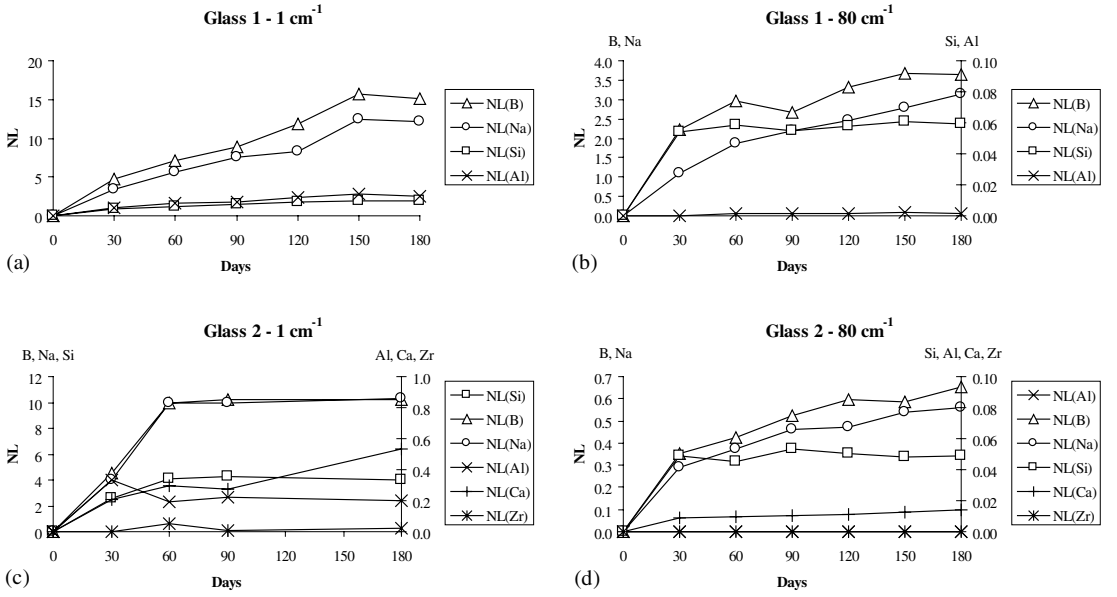

Fig. 2. Normalized mass losses (g/m^2) versus time of the elements liberated by the glasses alteration in pure water at 363 K ((a) and (b): glass 1, (c) and (d): glass 2) (error: 15%).

error is mainly due to the uncertainty about the S/V ratio variation during the glass dissolution). Silicon and aluminium were released congruently among each other at 1 cm^{-1}; however at 80 cm^{-1}, silicon leached from the glass faster than aluminium. One might speculate that, in the latter case, Al is incorporated in the secondary products.

The measured elemental concentrations in the glass 2 leachates at 1 and 80 cm^{-1} have been reported in Table 5. The pH had the same evolution as for the glass 1. At $S/V = 80$ cm^{-1}, the concentrations of boron, sodium and calcium increased regularly, whereas, at $S/V = 1$ cm^{-1}, they remained almost constant after 60 days (Fig. 1(c) and (d)). The silicon and aluminium concentrations

Table 5
Experimental results of the glass 2 static alteration at 1 and 80 cm^{-1} (363 K, pure water)

Days	pH	Concentration (mmol/l)						Normalized mass loss ($g\,m^{-2}$)					
		Si	Al	B	Na	Ca	Zr	NL(Si)	NL(Al)	NL(B)	NL(Na)	NL(Ca)	NL(Zr)
Glass 2, $S/V = 1$ cm^{-1}													
30	8.53	2.00	0.034	1.90	1.33	0.015	4.9×10^{-5}	2.54	0.34	4.54	4.03	0.207	0.002
60	8.87	2.79	0.016	3.57	2.82	0.019	9.8×10^{-4}	4.13	0.19	9.91	9.93	0.298	0.051
90	8.91	2.89	0.019	3.65	2.82	0.018	2.0×10^{-4}	4.30	0.22	10.19	10.00	0.275	0.010
180	8.92	2.70	0.017	3.66	2.92	0.034	4.3×10^{-4}	4.02	0.20	10.24	10.35	0.534	0.023
Glass 2, $S/V = 80$ cm^{-1}													
30	9.10	3.62	5.8×10^{-3}	13.87	9.01	0.063	1.2×10^{-4}	0.049	0.001	0.353	0.291	0.009	0.000
60	8.99	3.32	8.9×10^{-3}	16.58	11.53	0.066	1.2×10^{-4}	0.045	0.001	0.423	0.373	0.009	0.000
90	8.93	3.90	7.6×10^{-3}	20.40	14.21	0.072	8.6×10^{-5}	0.053	0.001	0.523	0.462	0.010	0.000
120	9.08	3.67	8.1×10^{-3}	23.28	14.47	0.079	8.8×10^{-5}	0.050	0.001	0.598	0.471	0.011	0.000
150	9.08	3.50	7.1 10^{-3}	22.81	16.52	0.087	9.7×10^{-5}	0.048	0.001	0.585	0.538	0.013	0.000
180	9.01	3.54	7.9×10^{-3}	25.31	17.22	0.100	2.2×10^{-4}	0.049	0.001	0.652	0.562	0.014	0.000

remained constant after 30 days at both S/V ratios (Fig. 1(c) and (d)). The zirconium concentrations remained about constant at 80 cm^{-1}, while they showed large variations at $S/V = 1$ cm^{-1}. As for glass 1, boron and alkali elements were released preferentially, with an alkali/silicon ratio increasing with the S/V ratio. Aluminium, calcium and zirconium were found strongly retained. The normalized mass losses of glass 2 elements have been plotted on Fig. 2(c) and (d). Boron and sodium were released congruently among each other at 1 cm^{-1}.

The evolution of NL values was fitted with the empirical $a \cdot x^b$ law [73] (glass 1 – 1 cm^{-1}: $0.45x^{0.69}$, $r^2 = 0.97$; glass 1 – 80 cm^{-1}: $0.87x^{0.28}$, $r^2 = 0.86$; glass 2 – 1 cm^{-1}: $1.28x^{0.44}$, $r^2 = 0.66$; glass 2 – 80 cm^{-1}: $0.11x^{0.35}$, $r^2 = 0.97$) and the plot of their derivatives gave directly the dissolution rate (Fig. 3) (Eq. (3)). As expected, the dissolution rate of the glasses altered at a high S/V ratio decreased faster than at $S/V = 1$ cm^{-1}.

The alteration rates after 180 days have been reported in Table 6 and were compared to literature data. The values obtained in this study at 80 cm^{-1} are very closed to those obtained by [73] for same glasses (Si–B–Na–Al and Si–B–Na–Al–Ca–Zr) altered in similar conditions (363 K, pure water, $S/V = 80$ cm^{-1}) (bold values in Table 6). They remain slightly higher than those measured for nuclear glasses but are of the same order of magnitude.

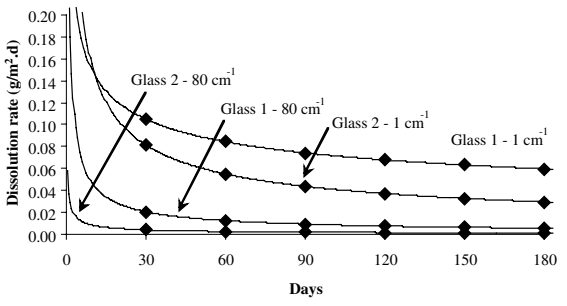

Fig. 3. Average dissolution rates (g/m^2 d) of the glasses altered in pure water at 363 K.

3.2. ASEM and ASTEM results

The direct observation of the altered glasses surface through ASEM allowed one to highlight the presence of an alteration layer, whatever the glass or the S/V ratio. The initial surface was preserved and traces of polishing remained visible, even after 180 days of leaching (Fig. 4(a) and b). Thus, this layer seems to be formed without the complete dissolution of glass. At 1 cm^{-1}, the surface of both glasses was fractured (Fig. 4(c) and (d)) and the attack of the pristine glass beneath the alteration layer is visible in Fig. 4(e) and (f).

The ASTEM observations showed that the structure of the glass 1 alteration gel was homogeneous at both S/V ratios (Fig. 5(a) and (b)). On the contrary, the gel of glass 2 was granular at $S/V = 1$ cm^{-1} (Fig. 5(c)), whereas it was dense at $S/V = 80$ cm^{-1} (Fig. 5(d)). Besides, at 1 cm^{-1}, two granular thin layers formed on glass 2, the most superficial layer being very thin (<0.1 μm) and the second thicker (Fig. 5(c)). The ASTEM analyses indicated that the superficial thin layer was highly enriched in zirconium, up to 50% in oxides weight.

The thicknesses of the alteration gels were measured through general ASEM microphotographs of monolith surface (Fig. 4(e) and (f)). They were generally quite thick on glass 1 (Fig. 6(a)), whereas, on glass 2, layers were thinner, especially at 80 cm^{-1} (Fig. 6(b)). These measurements were then compared to the layer thicknesses estimated from the solutions compositions

Table 6
Advanced dissolution rate ($g\,m^{-2}\,d^{-1}$) of different glasses altered in static mode in pure water at 363 K

Refs.	Glass	S/V (cm^{-1})	Time (days)	Rate ($g\,m^{-2}\,d^{-1}$)	pH	C(Si) (ppm)	log(Si_{tot})
[73]	Si–B–Na	1	180	0.35	9.06	288	−2.30
	Si–B–Na	80	180	2×10^{-2}	9.2	319	−2.26
[43]/[73]	Si–B–Na	4	7–14	0.35	8.86	274	−2.33
[73]	Si–B–Na–Al	80	273	$\mathbf{5\times10^{-3}}$	8.91	182	−2.50
[84]	Si–B–Na–Al	80	365	$\mathbf{3.2\times10^{-3}}$	8.9	200	−2.46
This work	Si–B–Na–Al	1	180	5.97×10^{-2}	8.86	49.3	−3.07
	Si–B–Na–Al	80	180	$\mathbf{5.6\times10^{-3}}$	8.99	121.9	−2.68
[73]	Si–B–Na–Al–Ca–Zr	80	273	$\mathbf{9\times10^{-4}}$	9.04	149	−2.59
[84]	Si–B–Na–Al–Ca–Zr	80	365	$\mathbf{4.9\times10^{-4}}$	9.0	164	−2.55
This work	Si–B–Na–Al–Ca–Zr	1	180	2.96×10^{-2}	8.92	78.4	−2.87
	Si–B–Na–Al–Ca–Zr	80	180	$\mathbf{1.3\times10^{-3}}$	9.01	101.8	−2.76
[35]	Basalt	0.1	8.9	0.327	8.595	10.2	−3.76
	Basalt	0.5	112	0.0011	8.625	18.8	−3.49
	Basalt	337	281	4.4×10^{-5}	9.96	32.4	−3.25
[69]	Basalt mod.	200	100	8×10^{-5}	9.3	15	−3.59
[74]/[16]	Nuclear	0.5	91–364	4.2×10^{-2}	8.43	33.4	−3.24
[72]	Nuclear	0.5	91–364	2×10^{-3}	9.3	30	−3.29
	Nuclear	0.5	56–364	11×10^{-3}	9.3	65	−2.95
	Nuclear	3.5	91–364	6×10^{-3}	9.6	60	−2.99
	Nuclear	80	56		10	180	−2.51
[71][a]	Nuclear	4	365	3×10^{-4}	8.4 ± 0.2	54.6	−3.03
	Nuclear	20	365	6×10^{-4}	8.8	120.1	−2.68
	Nuclear	80	365	6×10^{-4}	9.1	343.3	−2.23
	Nuclear	200	365	$<1\times10^{-4}$	9.5	166.3	−2.54
[73]	Nuclear	0.1	60–90	7.1×10^{-2}	9.04	28.75	−3.31
	Nuclear	1	60–90	1.7×10^{-3}	8.96	31.9	−3.26
	Nuclear	10	60–90	1×10^{-3}	9.03	42.6	−3.13
[42]	Nuclear	4		≈0.009			
	Nuclear	200		$<10^{-4}$			
[70]	Nuclear	0.5	61	≈0.013	8.92	25.6	−3.36
[47]	Nuclear	0.1	21–300	7.0×10^{-4}	8.57	21.1	−3.44
[68]	Nuclear	0.5	84	$<10^{-3}$	8.75	34.6	−3.22
[75]	Nuclear	12	548	2.7×10^{-3}	9.90	130.8	−2.65
[75]	Nuclear	12	548	3.3×10^{-4}	9.74	86	−2.83

[a] In Volvic water.

(Eq. (4)). Both methods were generally in good agreement except in the case of the glass 1 at 1 cm^{-1}, where the ASEM measurements were probably over-estimated. This over-estimation is probably due to the measurement method since the thickness was measured directly on ASEM microphotographs of the sample, at place where the layer thickness was apparent, as on Fig. 4(e). These conditions imply significant uncertainties.

3.3. Evolution of the alteration gel composition

The chemical composition of the alteration gel was evaluated by three different methods: direct analysis through ASEM and through ASTEM, and calculation from the solutions compositions.

In order to deduce the gel composition from the solutions composition, it was assumed that all the boron

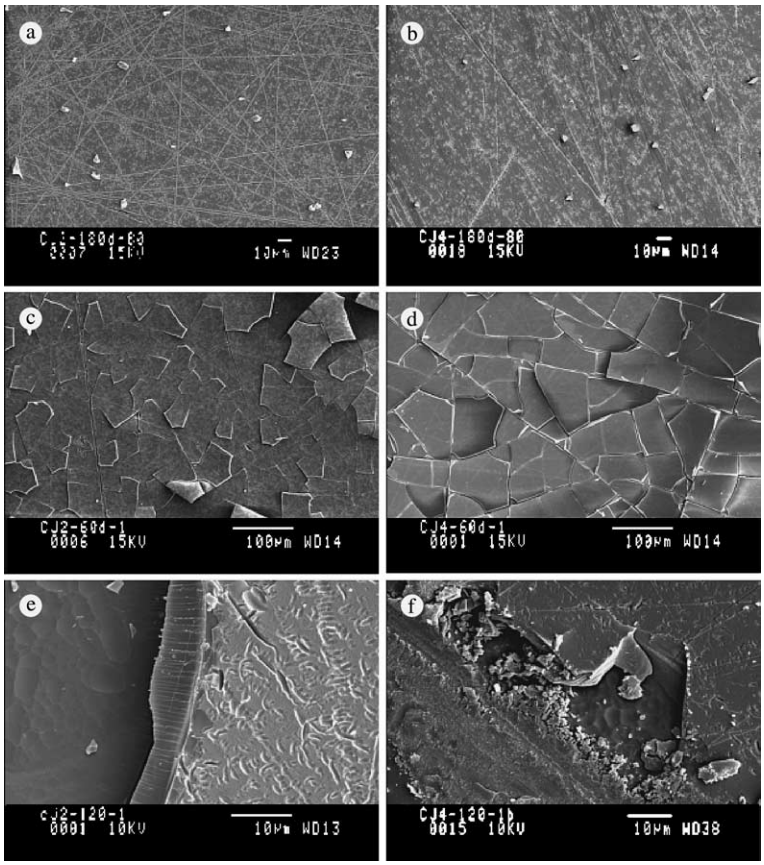

Fig. 4. Microphotographs (ASEM) of the surface of: (a) the glass 1 and (b) the glass 2 at 80 cm^{-1} altered 180 days (c) the glass 1 and (d) the glass 2 at 1 cm^{-1} altered 60 days (e) the glass 1 and (f) the glass 2 at 1 cm^{-1} altered 120 days, in pure water at 363 K.

was totally released in solution. The gel composition could then be calculated from the difference between the effectively released amount of the elements in solution and what this would have been considering the complete glass destruction, for the same released amount of boron.

$$n_{i,\mathrm{eq-glass}} = n_{\mathrm{B,sol}} \cdot (f_{i,\mathrm{glass}}/f_{\mathrm{B,glass}}),$$

$$n_{i,\mathrm{gel}} = n_{i,\mathrm{eq-glass}} - n_{i,\mathrm{sol}},$$

with $n_{\mathrm{B,sol}}$, the boron amount in solution (mol); $f_{i,\mathrm{glass}}$, the molar fraction of element '*i*' in glass; $n_{i,\mathrm{eq-glass}}$, the equivalent amount of element '*i*' if the glass would have dissolved completely without the formation of secondary products; $n_{i,\mathrm{gel}}$, amount of element '*i*' in gel.

The high solubility and mobility of sodium involved a great uncertainty of about 5% in oxides weight percentages on the ASEM and ASTEM analyses. Despite this, the results obtained with the three methods were in good agreement (Fig. 7). The important feature of these results is that the gel still contains noticeable amount of sodium. Moreover, the global composition of the gel was fairly constant during the alteration for each set of experiments except for the case of the glass 1 at 80 cm^{-1}, for which the sodium content decreased slightly with time. Besides, the alteration gel had similar mean composition for both S/V values in the case of the glass 1, whereas it changed according to the S/V ratio in the case of the glass 2 (Table 7).

4. Discussion and modelling

4.1. Silicon saturation state in the solution

The comparison between the silicon concentration and the solubility limits of amorphous silica, chalcedony and quartz, estimated at 363 K (Table 3) and at the mean experimental pH measured at 1 and 80 cm^{-1}, has been plotted on Fig. 8.

For the glass 1, the silicon concentrations reached two very different final values according to the S/V ratios. Thus, at 1 cm^{-1}, the silicon concentrations remained close to the quartz solubility, whereas at

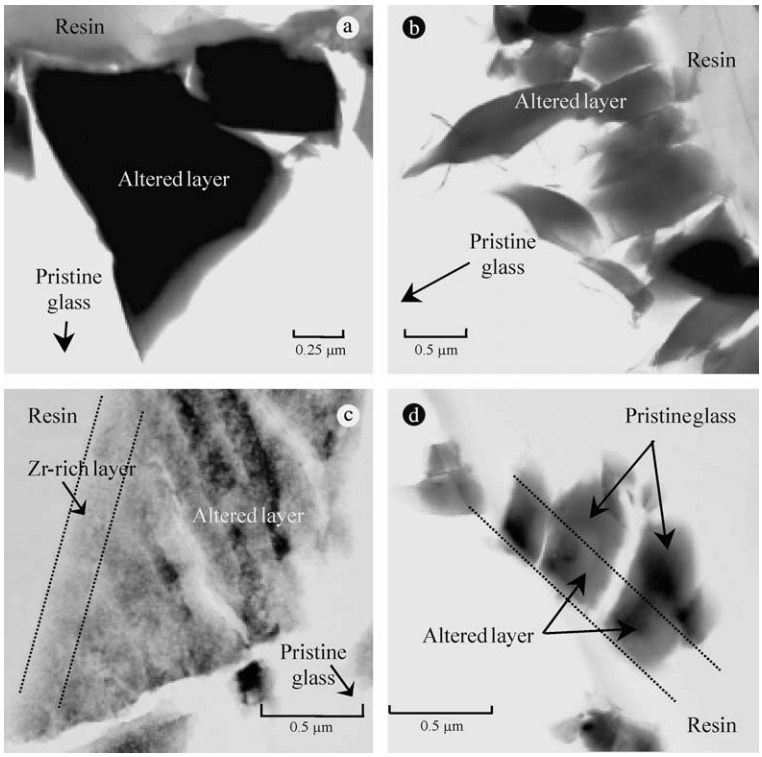

Fig. 5. Ultra-microtomic thin sections observed by ASTEM: (a) the glass 1 at 1 cm^{-1} altered 120 days, (b) the glass 1 at 80 cm^{-1} altered 180 days, (c) the glass 2 at 1 cm^{-1} altered 120 days and (d) the glass 2 at 80 cm^{-1} altered 120 days.

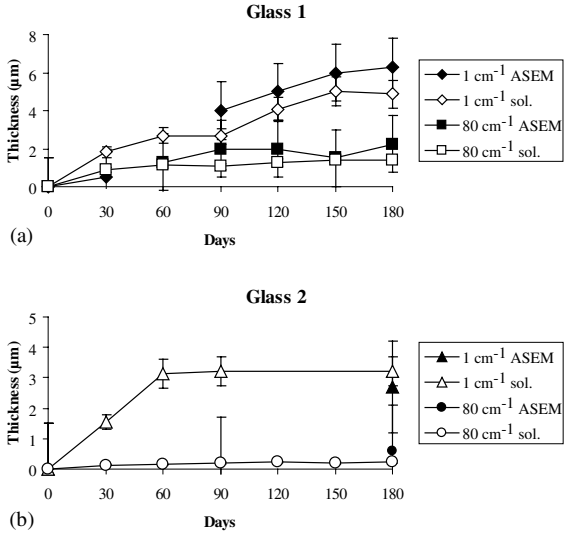

Fig. 6. Thicknesses of the alteration gel measured through ASEM (solid marks) (error: 1.5 μm) and estimated from the solutions compositions (empty marks) (error 15%) for the glass 1 (a) and the glass 2 (b).

80 cm^{-1}, they were higher than the chalcedony solubility (Fig. 8(a)). When considering the glass 2, the silicon concentrations obtained at 1 and 80 cm^{-1} were close and slightly higher than the chalcedony solubility (Fig. 8(b)).

The silicon concentration may be controlled by the following processes:

1. kinetic control by the glass dissolution rate (no precipitation of silicate),
2. kinetic control by the glass dissolution rate modified by the secondary silicated phase(s) formation,
3. control by a thermodynamic equilibrium with respect to the alteration gel only (the alteration gel should then be protective and does not allow direct contact between the hydrated glass surface and the solution, this case may thus, under certain conditions, correspond to the affinity control by the alteration gel solubility),
4. control by a thermodynamic equilibrium between the dealkalised hydrated glass surface (below the gel layer) and the solution (this would then correspond to the affinity control with respect to the dissolving phase but the solution would be supersaturated with respect to the alteration gel),
5. control by a mutual thermodynamic equilibrium between the dealkalised/hydrated glass surface, the alteration gel and the solution (this would also correspond

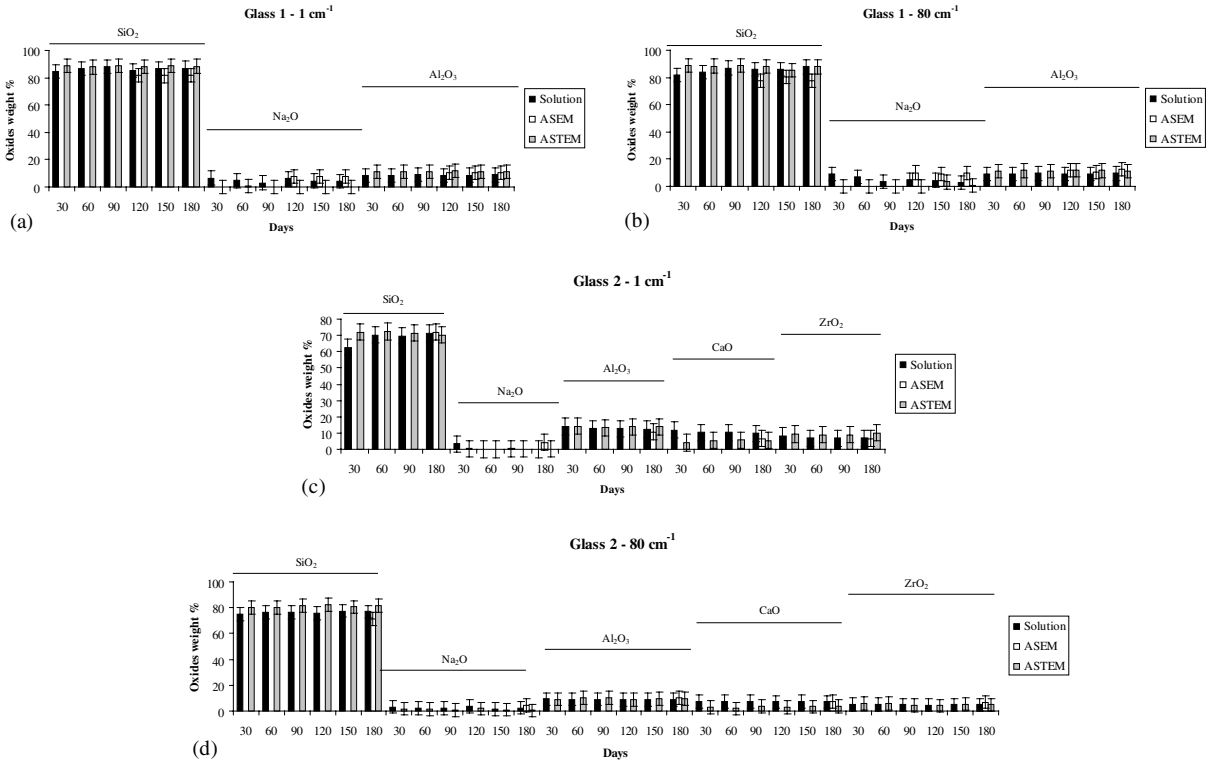

Fig. 7. Composition of the alteration layer composition, measured by ASEM and ASTEM, and estimated from the solution analyses (oxides weight%) (error: 5% of oxides weight).

Table 7
Mean chemical compositions of the alteration gels simulated by using different end-members and deduced from the solution analyses (oxides wt%)

			SiO_2	Na_2O	Al_2O_3	CaO	ZrO_2
Glass 1 1 cm^{-1}	Experiment		86.4	4.9	8.7	–	–
	Simulation	Oxides	88.11	–	11.89	–	–
		Hydroxides	88.17	–	11.83	–	–
		Metasilicates	88.11	–	11.89	–	–
Glass 1 180 cm^{-1}	Experiment		85.5	5.2	9.3	–	–
	Simulation	Oxides	90.14	–	9.86	–	–
		Hydroxides	90.14	–	9.86	–	–
		Metasilicates	90.14	–	9.86	–	–
Glass 2 1 cm^{-1}	Experiment		68.5	1.0	12.8	10.5	7.2
	Simulation	Oxides	80.49	–	12.50	–	7.01
		Hydroxides	80.94	–	12.27	–	6.78
		Metasilicates	75.41	–	10.82	7.79	5.98
Glass 2 80 cm^{-1}	Experiment		76.3	2.5	9.0	7.3	4.9
	Simulation	Oxides	85.06	–	9.72	–	5.23
		Hydroxides	85.03	–	9.73	0.03	5.20
		Metasilicates	79.04	–	8.90	7.30	4.76

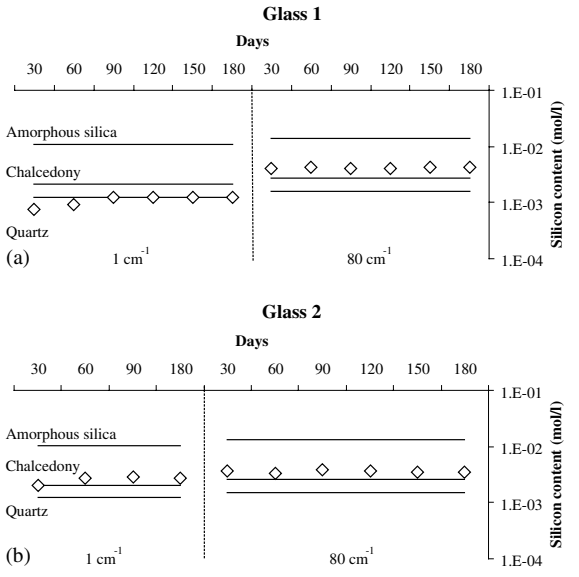

Fig. 8. Silicon contents (mol/l) versus the alteration time (days). The experimental values (empty mark) and the solubility limits of amorphous silica, chalcedony or quartz, calculated at 363 K according to the experimental mean pH: (a) glass 1 and (b) glass 2.

to affinity control with respect to the dissolving phase but also to global equilibrium of all reaction products) and

6. over-saturation of the solution with respect to both the alteration gel and the hydrated glass due to fast dissolution kinetics.

If a thermodynamic equilibrium is supposed for all time steps (cases 3–5), the evolution of the silicon content in the solution in the course of our experiments would indicate that the gel structure, and/or the gel composition or the composition of the hydrated glass surface evolves with the alteration time. Assuming equilibrium with pure silica polymorph, this corresponds to a gel (and/or a hydrated glass surface) having thermodynamic properties between chalcedony and amorphous silica, except for the glass 1 at 1 cm^{-1} where the gel (and/or a hydrated glass surface) would have quartz-like properties. Alternatively, it may be assumed that saturation has not yet been achieved for chalcedony for glass 1 at low S/V ratio (cases 1 and 2).

An effect of the S/V ratio on the silicon concentration is observed in the case of the R7T7 glass. Indeed, Fig. 9 shows the silicon concentrations measured by different authors (Table 6) at the end (>6 months) of static R7T7 alteration experiments at 363 K versus the S/V ratios used. At the end of these experiments, the silicon concentrations were then considered as being constant and stable. They spread over a large interval

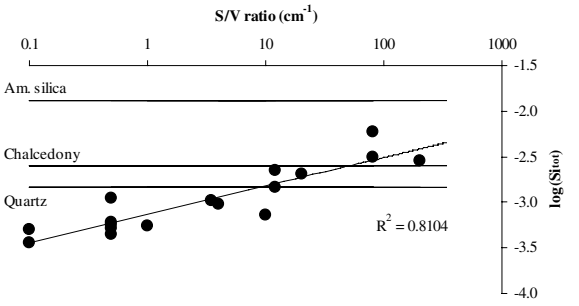

Fig. 9. $\log(Si_{tot})$ versus S/V ratio (cm^{-1}) measured at high reaction progress of R7T7 glass dissolution (Table 6). Solubilities of amorphous silica, chalcedony and quartz have been reported considering a mean pH of 9.

$(-3.5 < \log[Si_{tot}] < -2.0)$ and tended to increase with the S/V ratio [79].

Without additional information on the gel and the hydrated glass composition, these literature results could be interpreted in two ways, with a mixed kinetic/thermodynamic or a thermodynamic argument:

(a) *Kinetic/thermodynamic* – if the accumulation of the dissolved silicon in the solution is slow (i.e., dissolution at a small S/V ratio), the structure of the alteration gel would assume a more thermodynamically stable configuration, leading to a lower silicon concentration (this argument applies only to the alteration gel, not to the hydrated glass). This interpretation is consistent with the observation of an apparent stabilisation of the silicon content by controlling phases, as suggested by Curti [75] based on experiments of nuclear glass (SON68) dissolution at 363 K with $S/V = 12$ cm^{-1} for 13 years. Indeed, the silicon concentration was close to chalcedony solubility during up to five years and then decreased to reach quartz solubility after five years and remained constant thereafter.

(b) *Thermodynamic* – the composition of the gel and/or the hydrated glass depends on the S/V ratio. At high S/V ratio, the gel is more Si-rich, having thermodynamic properties close to those of chalcedony, whereas at low S/V ratio, the gel incorporates more metal ions, decreasing its solubility.

Finally, a combination of these arguments is also possible.

4.2. Numerical simulation of silicon content in solution

So as to estimate the effect of the thermodynamic stability of the siliceous secondary products on the solution concentrations achieved during glass corrosion, the alteration gel has been represented with a solid

solution by using three different siliceous end-members. Fig. 10(a) and (b) show the three simulated curves corresponding to the three tested siliceous end-members: amorphous silica (the less thermodynamically stable), quartz (the most stable) and chalcedony (of medium stability), for both glasses considered. The other end-members are constituted by hydroxides (Table 2), whose solubility constants have been reported in Table 3. On Fig. 10, the reaction progress is represented by the boron concentration in the solution, since it increases with the alteration time, without boron being noticeably reincorporated in the secondary products.

The simulated curves show the effect of the thermodynamic stability of the siliceous end-member on the silicon concentrations at equilibrium: the more stable the end-member, the more stable the gel and the lower the silicon content. The relative stability of the end-members is amorphous silica < chalcedony < quartz and thus the silicon increasing concentration follows the same order, whatever the glass dissolution simulated.

For the glass 1 (Fig. 10(a)), the best agreement was achieved at 1 cm^{-1} with quartz and chalcedony as end-member. At 80 cm^{-1}, the experimental values were slightly higher than those simulated with chalcedony as end-member. The alteration of the glass 2, which has a more complex composition, led to silicon concentrations close to but slightly higher than those obtained with chalcedony simulation, whatever the S/V ratio.

On Fig. 10 have been also reported the simulated curves obtained when no solid solution can form, what thus corresponds only to the increase of silicon concentration due to the glass dissolution, without formation of siliceous secondary products. When glass dissolved without forming minerals or gel, the silicon concentrations increased sharply and the difference between concentrations, corresponding to simulation with and without the alteration gel formation, can exceed one order of magnitude, especially at high S/V ratio. Therefore, these curves indicate the fundamental incidence of the gel formation on the evolution of the silicon concentration.

To study the effect of the choice of the other end-members (Al, Na, Ca, Zr) on calculations, simulations were also carried out by using oxides or metasilicates, the siliceous end-member being chalcedony (Table 3 and Fig. 11). When considering the dissolution of glass 1, the simulations results were similar whatever the set of end-members used, due to the absence of Zr and Ca in the glass. For the glass 2, the hydroxides end-members set gave the best agreement, even if the three curves were close to each other. The comparison of the silicon contents in solution measured experimentally or simulated with chalcedony and hydroxide shows a mean relative difference lower than 35% what can be considered as a good agreement.

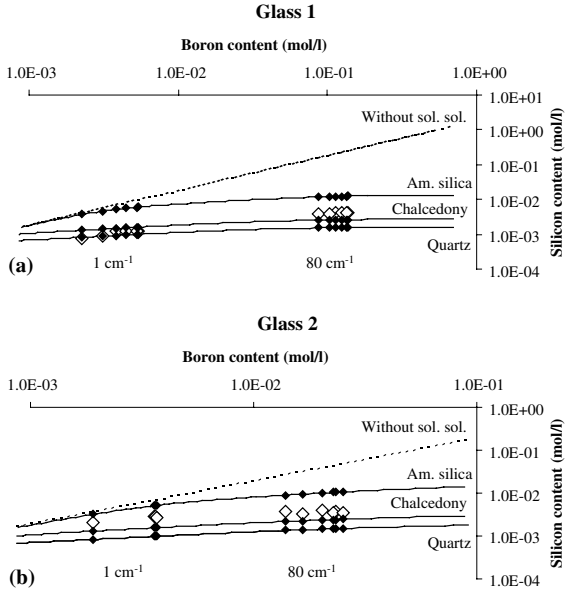

Fig. 10. Silicon contents versus boron contents (mol/l). Experimental values (empty mark) and simulated values (solid mark) by using a solid solution having amorphous silica, chalcedony or quartz as siliceous end-member, and hydroxides as other end-members: (a) glass 1 and (b) glass 2.

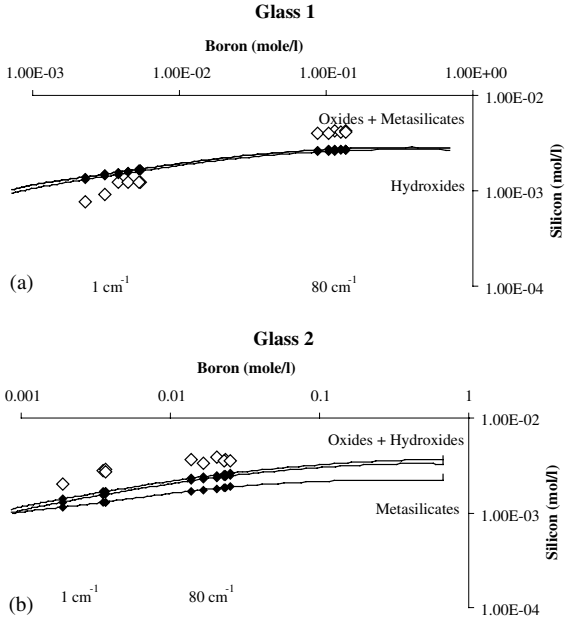

Fig. 11. Silicon contents versus boron contents (mol/l). Experimental values (empty mark) and simulated values (solid mark) by using a solid solution having chalcedony as siliceous end-member and oxides, hydroxides or metasilicates as other end-members: (a) glass 1 and (b) glass 2.

These results illustrate the complexity of the phenomena, which can take place when the S/V ratio varies (glass 1) but they also show that it is clearly possible to reproduce with a good agreement the experimental silicon concentrations by using a solid solution model to simulate the gel formation and by using only thermodynamic data coming from literature (i.e. not fitted). Furthermore, it is fundamental to note that the agreement between the experiments and the simulation justifies the description of the alteration gel in simulation by considering a total dissolution process followed by an in situ precipitation of the gel at thermodynamic equilibrium with the solution.

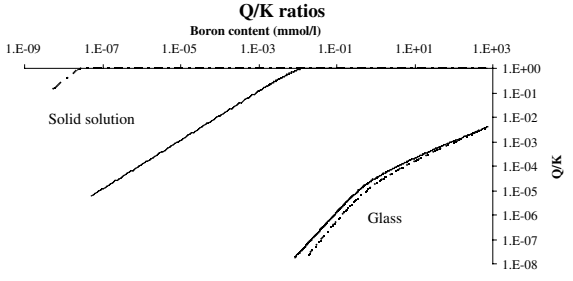

Fig. 12. Q/K ratios of the solid solutions, having chalcedony and hydroxides as end-members, and of both glasses (continuous line: glass 1 and dotted line: glass 2) versus the boron contents.

On Fig. 12 has been reported the Q/K ratio of the solid solutions, having chalcedony and hydroxides as end-members, and of both glasses. The gel simulated precipitation occurs at the very first steps of the glass dissolution as it might be the case when a glass is immersed in water and forms immediately an altered layer. Fig. 12 also shows that glasses remained far below their solubility limit. The incidence of the affinity between the gel (and/or the hydrated glass) versus the solution upon the kinetics of the glass dissolution will be developed in a forthcoming article.

4.3. Simulation of gel composition

The simulated compositions of the alteration gel layer have been plotted Fig. 13. At low S/V ratio, the gel composition varied a little as the reaction proceeds, whereas, at high S/V ratio, the gel composition remained constant, whatever the glass considered. The mean compositions of the gel layers have been reported in Table 7.

For glass 1, the gel mean composition was very similar for the same S/V ratio, whatever the end-members used, but it varied slightly according to the S/V ratio and, at high S/V ratio, the gel was enriched in silicon and impoverished in aluminium.

In the case of glass 2, the choice of the end-members, used to simulate the gel layer, greatly influenced the gel composition, whatever the S/V ratio. Indeed, with metasilicates as end-members, the gel layer contained

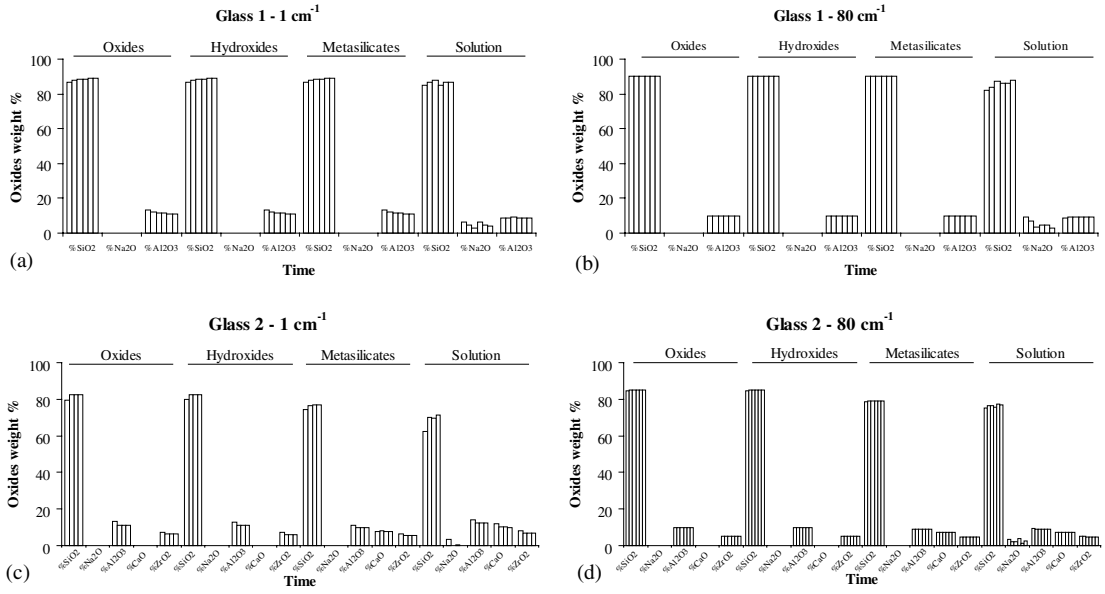

Fig. 13. Composition of the simulated and deduced from solution alteration gels (oxides wt%) according to the choice of the end-members (oxides, hydroxides and metasilicates) and the alteration time (from left to right: 30, 60, 90, 120, 150 and 180 days, except for glass 2 at 1 cm^{-1}: 30, 60, 90 and 180 days) (a and b: glass 1, c and d: glass 2).

significant amounts of calcium, whereas it is not the case by using oxides or hydroxides as end-members. The gel simulated layer composition also varied with the S/V ratio as it was the case experimentally. Besides, the gel layer became slightly enriched in silicon with increasing S/V ratio and impoverished in aluminium and zirconium as it was also observed from the experimental solution data.

These globally constant gel compositions conceal great variations in molar content (Fig. 14). Indeed, the amounts of elements in the gel increased significantly as the reaction proceeds, what corresponds to the gel growth in the course of the alteration.

On the whole, the results obtained by KINDIS program for simulating the gel layer composition are similar to the main tendencies obtained for the experimental gel layer. A very good agreement with the experimental measurements was obtained for silicon: simulated gel composition models the experimental gel composition with an agreement being between 80% and 99% according to the glass and the S/V ratio, for aluminium (between 80% and 99.8%) and for zirconium (98%), especially at 80 cm^{-1}. The simulation of the calcium content was particularly good when metasilicates were used (94%).

The main discrepancy between the experimental and the simulated compositions of the alteration layers concerned essentially the sodic end-members. Indeed, the high solubility of the sodic end-members considered in this study (Table 3) did not allow their incorporation into the solid solution, whatever the glass or the S/V ratio, whereas the experimental gel layers contained significant amounts of sodium (Table 7), notably for the glass 1 (≈5%).

The presence of sodium in the alteration gel layer of nuclear glass has been reported in literature [76,77] and these authors explained the observed Na content by the structure of the gel. Indeed, in the alteration gel layer, Al atoms are likely to have a fourfold coordination (AlO_4^-) and Zr atoms a sixfold coordination (ZrO_6^{2-}) [76]. This structure involves an excess of charges and thus requires the presence of compensators such as alkaline and alkaline earth elements for the charge balance. Such effect might be taken into account in the future calculations by using sodium–aluminium silicates as Na-rich end-members. The glass composition and its alkaline and alkaline earth elements content could then explain why a glass with large amounts of Na, Al and Zr but without Ca forms a gel layer rich in Na, which compensates the AlO_4^- and ZrO_6^{2-} charges, whereas a glass containing high amounts of Ca and Na tends to liberate Na, since Ca is then used as charge compensator.

In our case, the alteration gel layers of glass 1 contain significant amounts of Na and Al (Table 7), which are equimolar on average, what would then probably correspond to the compensation of AlO_4^- charges by Na^+ [83]. The glass 2 alteration gel layers contain very low amounts in Na but high in Ca, what could signify that Ca is then the main compensator of charge balance [73].

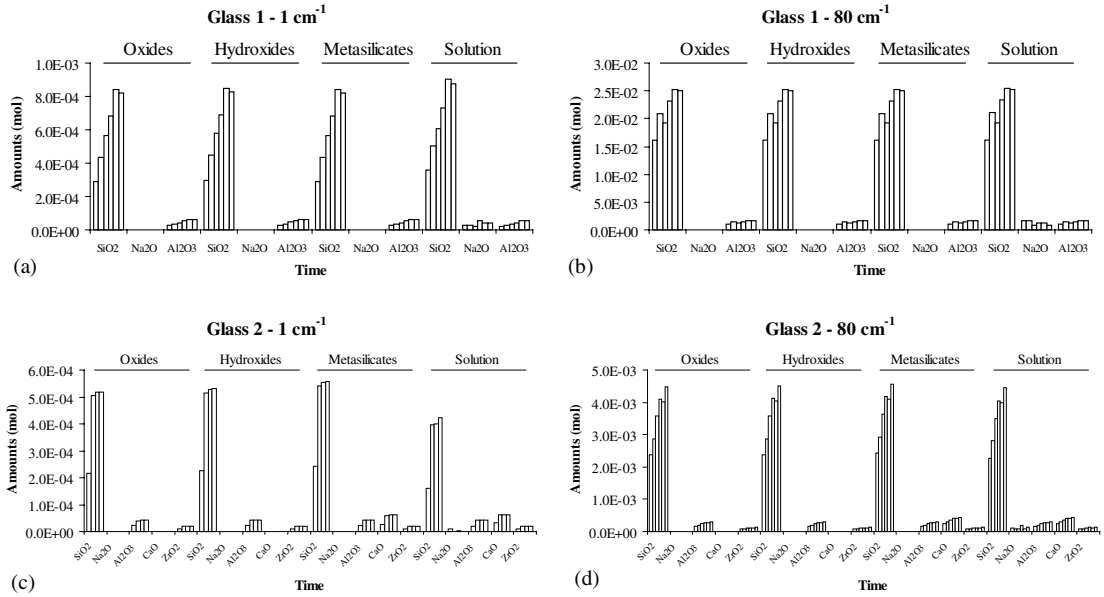

Fig. 14. Molar compositions of the simulated alteration gels according to the end-members and molar composition of the gels deduced from the solution analyses (mol) versus the alteration time (from left to right: 30, 60, 90, 120, 150 and 180 days, except for glass 2 at 1 cm^{-1}: 30, 60, 90 and 180 days).

5. Conclusion

Whatever the glass or the S/V ratio considered, an alteration layer (gel) developed on the glass surface during alteration. These gels did not consist of identifiable minerals but of amorphous products, being not very porous and not easily distinguishable from pristine glass except by their composition. However, in the case of glass 2, Zr-rich layers were observable in the external part of the alteration gel. They are probably the relics of the first stages of the dissolution, when Zr was the first secondary product to precipitate. It seems that thereafter Zr was incorporated in the structure of the alteration gel.

The silicon concentrations of the solutions varied obviously according to the time and to the glass composition but also, for the same glass, according to the S/V ratio. They were lower at 1 cm^{-1} than at 80 cm^{-1}, especially in the case of glass 1. We think that these observations reflect transitory situations and, at long term, the silicon concentrations may decrease towards the lowest values, at equilibrium with quartz, as suggested by promising experiments of Curti et al. [75].

The agreement between the simulated and the experimental gel layer compositions was very good, especially for sparingly soluble elements. This agreement is all the more noteworthy since we considered in the model that the gel layer was formed by precipitation of a solid solution at equilibrium with respect to the solution, after total dissolution of the vitreous network. This modelling did not reproduce strictly the experiments, since the experimental gel layers were quite obviously a residual reorganized hydrated glass. All of this shows that a thermodynamic model allows one to foresee the stability of the secondary phases without necessary taking into consideration all of the actual mechanisms.

Acknowledgements

This study could not have been done without the financial support of the European Commission (GLASTAB project, contract no. FIKW-CT-2000-00007). This is the contribution no. 2003.401-UMR7517 of the EOST/CGS. The ASTEM analyses were able to be carried out thanks to G. Morvan and A. Arth from the CGS. We especially thank the reviewers and E. Curti.

References

[1] G. Malow, R.C. Ewing, in: Materials Research Society Symposium Proceedings, vol. 3, 1981, p. 315.
[2] C.D. Byers, M.J. Jercinovic, R.C. Ewing, K. Keil, Materials Research Society Symposium Proceedings, vol. 44, 1985, p. 583.
[3] B. Grambow, M.J. Jercinovic, R.C. Ewing, C.D. Byers, Materials Research Society Symposium Proceedings, vol. 50, 1985, p. 263.
[4] W. Lutze, G. Malow, R.C. Ewing, M.J. Jercinovic, K. Keil, Nature 314 (6008) (1985) 252.
[5] R.C. Ewing, M.J. Jercinovic, Materials Research Society Symposium Proceedings, vol. 84, 1987, p. 67.
[6] T. Murakami, T. Banba, M.J. Jercinovic, R.C. Ewing, Materials Research Society Symposium Proceedings, vol. 127, 1989, p. 65.
[7] A. Abdelouas, J.L. Crovisier, W. Lutze, B. Fritz, A. Mosser, R. Müller, Clays Clay Minerals 42 (5) (1994) 526.
[8] J. Caurel, E. Vernaz, D. Beaufort, Materials Research Society Symposium Proceedings, vol. 176, 1990, p. 309.
[9] J.-L. Crovisier, E. Vernaz, J.L. Dussossoy, J. Caurel, Appl. Clay Sci. 7 (1992) 47.
[10] S.R. Gislason, H.P. Eugster, Geochim. Cosmochim. Acta 51 (1987) 2827.
[11] J.-L. Crovisier, H. Atassi, V. Daux, J.-P. Eberhart, Comptes Rendus de l'Académie des Sciences, Paris – Série IIa: Sciences de la Terre et des Planètes 310 (Série II) (1990) 941.
[12] J.L. Crovisier, J.H. Thomassin, T. Juteau, J.P. Eberhart, J.C. Touray, P. Bailli, Geochim. Cosmochim. Acta 47 (1983) 377.
[13] J.-H. Thomassin, J.-L. Nogues, J.-C. Touray, Comptes Rendus de l'Académie des Sciences, Paris, Série IIa: Sciences de la Terre et des Planètes 297 (1983) 857.
[14] R. Wallace, G. Wicks, Materials Research Society Symposium Proceedings, vol. 15, 1983, p. 23.
[15] S. Fillet, J.L. Nogues, E. Vernaz, N. Jacquet-Francillon, Materials Research Society Symposium Proceedings, vol. 50, 1985, p. 211.
[16] J.L. Nogues, E.Y. Vernaz, N. Jacquet-Francillon, Materials Research Society Symposium Proceedings, vol. 44, 1985, p. 89.
[17] J.-H. Thomassin, J.-L. Crovisier, J.-C. Touray, T. Juteau, F. Boutonnat, Bulletin de la Société Géologique de France 1 (2) (1985) 217.
[18] G. Berger, J. Schott, M. Loubet, Earth Planet. Sci. Lett. 84 (1987) 431.
[19] R. Cowan, R.C. Ewing, Materials Research Society Symposium Proceedings, vol. 127, 1989, p. 49.
[20] J.-L. Crovisier, H. Atassi, V. Daux, J. Honnorez, J.C. Petit, J.P. Eberhart, Materials Research Society Symposium Proceedings, vol. 127, 1989, p. 41.
[21] T.A. Abrajano, J.K. Bates, A.B. Woodland, J.P. Bradley, W.L. Bourcier, Clays Clay Minerals 38 (5) (1990) 537.
[22] M.J. Jercinovic, S.A. Kaser, R.C. Ewing, W. Lutze, Materials Research Society Symposium Proceedings, vol. 176, 1990, p. 355.
[23] M.J. Jercinovic, K. Keil, M.R. Smith, R.A. Schmitt, Geochim. Cosmochim. Acta 54 (1990) 2679.
[24] J.-C. Petit, G. Della Mea, J.-C. Dran, M.-C. Magonthier, P.A. Mando, A. Paccagnella, Geochim. Cosmochim. Acta 54 (1990) 1941.
[25] J.-L. Crovisier, J. Honnorez, B. Fritz, J.-C. Petit, Appl. Geochem. (Suppl. 1) (1992) 55.
[26] V. Daux, J.L. Crovisier, C. Hemond, J.C. Petit, Geochim. Cosmochim. Acta 58 (22) (1994) 4941.
[27] W.L. Gong, L.M. Wang, R.C. Ewing, E. Vernaz, J.K. Bates, W.L. Ebert, J. Nucl. Mater. 254 (1998) 249.

[28] X. Le Gal, J.-L. Crovisier, F. Gauthier-Lafaye, J. Honnorez, B. Grambow, Comptes Rendus de l'Académie des Sciences, Paris – Série IIa: Sciences de la Terre et des Planètes 329 (3) (1999) 175.
[29] J.-L. Crovisier, B. Fritz, B. Grambow, J.P. Eberhart, Materials Research Society Symposium Proceedings, vol. 50, 1985, p. 273.
[30] G. Berger, J. Schott, C. Guy, Chem. Geol. 71 (1988) 297.
[31] J.-L. Crovisier, T. Advocat, J.C. Petit, B. Fritz, Materials Research Society Symposium Proceedings, vol. 127, 1989, p. 57.
[32] L. Michaux, E. Mouche, J.-C. Petit, B. Fritz, Appl. Geochem. (Suppl. 1) (1992) 41.
[33] S.R. Gislason, D.R. Veblen, K.J.T. Livi, Geochim. Cosmochim. Acta 57 (1993) 1459.
[34] T. Advocat, P. Jollivet, J.L. Crovisier, M. Del Nero, J. Nucl. Mater. 298 (2001) 55.
[35] I. Techer, T. Advocat, J. Lancelot, J.-M. Liotard, Chem. Geol. 176 (2001) 235.
[36] P. Aagaard, H.C. Helgeson, Am. J. Sci. 282 (1982) 237.
[37] B. Grambow, Materials Research Society Symposium Proceedings, vol. 44, 1985, p. 15.
[38] S. Gin, Materials Research Society Symposium Proceedings, vol. 412, 1996, p. 189.
[39] V. Daux, C. Guy, T. Advocat, J.-L. Crovisier, P. Stille, Chem. Geol. 142 (1997) 109.
[40] B.P. McGrail, W.L. Ebert, A.J. Bakel, D.K. Peeler, J. Nucl. Mater. 249 (2–3) (1997) 175.
[41] G. Leturcq, G. Berger, T. Advocat, E. Vernaz, Chem. Geol. 160 (1999) 39.
[42] T. Advocat, J.L. Chouchan, J.L. Crovisier, C. Guy, V. Daux, C. Jégou, S. Gin, E. Vernaz, Materials Research Society Symposium Proceedings, vol. 506, 1998, p. 63.
[43] C. Jégou, S. Gin, F. Larché, J. Nucl. Mater. 280 (2000) 216.
[44] S.A. Carrol, W.L. Bourcier, B.L. Phillips, Materials Research Society Symposium Proceedings, vol. 333, 1994, p. 533.
[45] W.L. Bourcier, D.W. Peiffer, K.G. Knauss, K.D. McKeegan, D.K. Smith, Materials Research Society Symposium Proceedings, vol. 176, 1990, p. 209.
[46] I. Techer, T. Advocat, J. Lancelot, J.-M. Liotard, J. Nucl. Mater. 282 (2000) 40.
[47] S. Gin, P. Jollivet, M. Mestre, M. Jullien, C. Pozo, Appl. Geochem. 16 (2001) 861.
[48] B. Grambow, R. Müller, J. Nucl. Mater. 298 (2001) 112.
[49] G. Ehret, J.L. Crovisier, J.P. Eberhart, J. Non-Cryst. Solids 86 (1986) 72.
[50] B. Madé, A. Clément, B. Fritz, Comptes Rendus de l'Académie des Sciences, Paris – Série IIa: Sciences de la Terre et des Planètes 310 (1990) 31.
[51] B. Madé, A. Clément, B. Fritz, Comput. Geosci. 20 (1994) 31.
[52] B. Madé, A. Clément, B. Fritz, Revue de l'Institut du Pétrole 49 (9) (1994) 1347.
[53] B. Fritz, Etude thermodynamique et modélisation des réactions hydrothermales et diagénétiques – Sciences Géologiques, Mémoires, Université Louis Pasteur, Strasbourg, vol. 65, 1981, p. 197.
[54] Y. Tardy, B. Fritz, Clay Mineral. 16 (1981) 361.
[55] A. Paul, J. Mater. Sci. 12 (1977) 2246.
[56] Y. Linard, Détermination des enthalpies libres de formation des verres borosilicatés. Application à l'étude de l'altération des verres de confinements de déchets radioactifs, PhD of the Institut de Physique du Globe de Paris, 2000, p. 265.
[57] H.C. Helgeson, J.M. Delany, H.W. Nesbitt, D.K. Bird, Am. J. Sci. A 278 (1978) 1.
[58] E.L. Shock, D.C. Sassani, M. Willis, D.A. Sverjensky, Geochim. Cosmochim. Acta 61 (5) (1997) 907.
[59] R.A. Robie, B.S. Hemingway, J.R. Fisher, Geol. Survey Bull. 1452 (1979) 456.
[60] E.L. Shock, H.C. Helgeson, D.A. Sverjensky, Geochim. Cosmochim. Acta 53 (1989) 2157.
[61] R.A. Robie, B.S. Hemingway, US Geol. Survey Bull. 2131 (1995) 461.
[62] V.I. Babushkin, G.M. Matveyev, O.P. Mchedlov-Petrossyan, Thermodynamics of Silicates, Springer-Verlag, Berlin, 1985, p. 459.
[63] C.F. Baes Jr., R.E. Mesmer, The Hydrolysis of Cations, John Wiley, New York, 1976, p. 489.
[64] D.D. Wagman, W.H. Evans, V.B. Parker, I. Halow, S.M. Bailey, R.H. Schumm, Selected values of chemical thermodynamic properties, Tables for the first thirty-four elements in the standard order of arrangement, NBS Technical Note, 270-3, 1968, p. 264.
[65] V.B. Parker, D.D. Wagman, W.H. Evans, Selected values of chemical thermodynamic properties. Tables for alkaline earth elements (elements 92 through 97 in the standard order arrangement), NBS Technical Note, 270-6, 1971, p. 106.
[66] E.L. Shock, H.C. Helgeson, Geochim. Cosmochim. Acta 52 (1988) 2009.
[67] W.L. Ebert, Phys. Chem. Glasses 34 (2) (1993) 58.
[68] S. Gin, I. Ribet, M. Couillard, J. Nucl. Mater. 298 (2001) 1.
[69] G. Leturcq, G. Berger, T. Advocat, C. Fillet, O. Halgand, E. Vernaz, Materials Research Society Symposium Proceedings, vol. 506, 1998, p. 199.
[70] S. Gin, C. Jégou, E. Vernaz, Appl. Geochem. 15 (2000) 1505.
[71] T. Advocat, Les mécanismes de corrosion en phase aqueuse du verre nucléaire R7T7. Approche expérimentale. Essai de modélisation thermodynamique et cinétique, PhD of the University Louis Pasteur, Strasbourg, 1991, p. 213.
[72] S. Fillet, Mécanisme de corrosion et comportement des actinides dans le verre nucléaire R7T7, PhD of the University of Montpellier, 1987, p. 338.
[73] C. Jégou, Mise en évidence expérimentale des mécanismes limitant l'altération du verre R7T7 en milieu aqueux. Critique et proposition d'évolution du formalisme cinétique, PhD of the University of Sciences and Techniques of Languedoc, Montpellier II, 1998, p. 224.
[74] J.-L. Nogues, Les mécanismes de corrosion des verres de confinement des produits de fission, PhD of the University of Sciences and Techniques, Montpellier, 1984, p. 322.
[75] E. Curti, Glass dissolution parameters: update for Entsorgungnachweis 2002, Nagra Technical Report 02-21, Wettingen, Switzerland, and PSI-Bericht, Paul Scherrer Institut, Villigen, Switzerland, 2003, in press.
[76] S. Ricol, Etude du gel d'altération des verres nucléaires et synthèse de gels modèles, PhD of the University Pierre et Marie Curie, Paris VI, 1995, p. 177.
[77] O. Zarembowitch-Déruelle, Etude in situ de la couche d'altération de verres, PhD of the University Pierre et Marie Curie, Paris VI , 1997, p. 186.

[78] G. Berger, C. Claparols, C. Guy, V. Daux, Geochim. Cosmochim. Acta 58 (22) (1994) 4875.
[79] E. Vernaz, S. Gin, C. Jégou, I. Ribet, J. Nucl. Mater. 298 (2001) 27.
[80] L.O. Werme, I. Björner, G. Bart, H.U. Zwicky, B. Grambow, W. Lutze, R. Ewing, C. Magrabi, J. Mater. Res. 5 (5) (1990) 1130.
[81] B. Grambow, in: D.E. Clark, B.K. Zoitos (Eds.), Corrosion of Glass, Ceramics and Ceramic Superconductors, Noyes Publisher, Park Ridge, New Jersey, 1992, p. 124.
[82] T. Advocat, J.L. Crovisier, E. Vernaz, G. Ehret, H. Charpentier, Materials Research Society Symposium Proceedings, vol. 212, 1991, p. 57.
[83] F. Angeli, T. Charpentier, S. Gin, J.C. Petit, Chem. Phys. Lett. 341 (2001) 23.
[84] S. Gin, S. Jégou, Tenth International Sympsosium on Water–Rock Interaction, Villasimius, Italy, 10–15 July 2001, p. 279.
[85] C. Jégou, S. Gin, F. Larché, J. Nucl. Mater. 280 (2000) 216.
[86] W. Hummel, U. Berner, E. Curti, F.J. Pearson, T. Thoenen, Nagra/PSI Chemical Thermodynamic Data Base 01/01. Universal Publisher/uPUBLISH.com. Available from: www.uPUBLISH.com/books/hummel.htm, 2002.
[87] H. Bilinski, M. Branica, L.G. Sillen, Acta Chem. Scand. 20 (1966) 853.